

1 **Mechanisms and effects of under-ice warming water in Ngoring**
2 **Lake of Qinghai-Tibet Plateau**

3 Mengxiao Wang ^{1,2}, Lijuan Wen ^{1*}, Zhaoguo Li ¹, Matti Leppäranta ³,
4 Victor Stepanenko ^{4,5}, Yixin Zhao ^{1,2}, Ruijia Niu ^{1,2}, Liuyiyi Yang ^{1,2} and
5 Georgiy Kirillin ⁶

6 ¹ Key Laboratory of Land Surface Process and Climate Change in Cold and Arid
7 Regions, Northwest Institute of Eco-Environment and Resources, Chinese Academy of
8 Sciences, 730000 Lanzhou, China

9 ² University of Chinese Academy of Sciences, 10049 Beijing, China

10 ³ Institute of Atmospheric and Earth Sciences, University of Helsinki

11 ⁴ Research Computing Center, Lomonosov Moscow State University, Moscow, Russia

12 ⁵ Moscow Center for Fundamental and Applied Mathematics, Moscow, Russia

13 ⁶ Department of Ecohydrology, Leibniz-Institute of Freshwater Ecology and Inland
14 Fisheries (IGB), Berlin, Germany

15 **Correspondence to: Lijuan Wen (wlj@lzb.ac.cn)*

16
17 **Abstract** The seasonal ice cover in lakes of the Qinghai-Tibet Plateau is a transient and
18 vulnerable part of the cryosphere, whose characteristics depend on the regional climate:
19 strong solar radiation in the context of the dry and cold environment. We use the first
20 under-ice temperature observations from the largest Tibetan freshwater lake Ngoring
21 and a one-dimensional lake model to quantify the mechanism of solar thermal
22 accumulation under ice, which relies on the ice optical properties and weather
23 conditions, as well as the effect of the accumulated heat on the land-atmosphere heat
24 exchange after the ice break-up. The model was able to realistically simulate the feature
25 of Ngoring Lake thermal regime: the “summer-like” temperature stratification with
26 temperatures exceeding the maximum density point of 3.98 °C across the bulk of the
27 water column. A series of sensitivity experiments revealed solar radiation was the major
28 source of under-ice warming and demonstrated that the warming phenomenon was
29 highly sensitive to the optical properties of ice. The heat accumulated under ice
30 contributed to the heat release from the lake to the atmosphere for 1-2 months after ice-
31 off, increasing the upward sensible and latent surface heat fluxes on average by ~50 W
32 m⁻² and ~80 W m⁻², respectively. Therefore, the delayed effect of heat release on the
33 land-atmosphere interaction requires an adequate representation in regional climate

34 modeling of the Qinghai-Tibet Plateau and other lake-rich alpine areas.

35

36 **1 Introduction**

37 Seasonal lake ice is a part of the cryosphere, gaining recent attention from
38 researchers due to its sensitivity to climate change (Kirillin et al., 2012; Sharma et al.,
39 2020). The duration of ice cover affects the stability and vertical mixing of lakes, as
40 well as the lake-atmosphere matter and energy exchange (Rösner et al., 2012; Efremova
41 et al., 2013; Ramp et al., 2015). Ice cover regulates lake biochemical indicators, such
42 as the concentration of dissolved oxygen, nitrogen, and phosphorus, changing the
43 biochemical reaction rate and affecting the water quality and distribution of aquatic
44 organisms (Weitere et al., 2010; Dokulil, 2013; Li et al., 2015a; Hardenbicker et al.,
45 2016). Shortening of the ice season has been observed worldwide (Sharma et al., 2019;
46 Dauginis and Brown 2021) and attributed to anthropogenic warming (Grant et al., 2021).
47 Future climate predictions indicated the accelerated reduction of seasonal lake ice,
48 especially pronounced in the lake-rich Arctic regions (Brown and Duguay 2011).
49 Global assessment of seasonal lake ice changes requires quantification of the major heat
50 sources and sinks on seasonal to climatic time scales. While the major prerequisite for
51 the ice cover development is sufficient long season with air temperature below the
52 freezing point of water, the heat budget of ice-covered lakes varies with latitude and
53 altitude, depending strongly on the available solar radiation, the latter being the major
54 source of heat for under-ice lake water (Kirillin et al., 2012). During the polar night in
55 the Arctic and temperate lakes covered by snow, the solar heating is minor and the
56 bottom sediment is the main heat source (Winter I according to Kirillin et al., 2012); at
57 later stages of the ice season (Winter II), as the snow melts, solar radiation becomes to
58 the main heat source governing thermal stratification and mixing under ice and the
59 melting process at the ice base (Kirillin et al., 2018, 2020). Further, lakes with seasonal
60 ice cover can be divided into cryomictic and cryostratified according to their maximum
61 depth, surface area, and wind speed (Yang et al., 2021). In dry and cold areas with little
62 snow, winter II can occupy the entire ice-covered period (Kirillin et al., 2012), making
63 solar radiation to be the major factor affecting the lake ice regime. The situation is
64 relevant to the alpine lakes.

65 In particular, the largest alpine lake system of the Qinghai-Tibet Plateau (TP), the
66 highest plateau on Earth with an average altitude of 4000-5000 m ensures a high amount
67 of solar radiation and low winter precipitation. The TP is covered by more than 1400
68 lakes with an area larger than 1 km², and the total lake area is more than 5×10^4 km²,
69 accounting for 57.2 % of that in China (Wan et al., 2016; Zhang et al., 2019). Recent

70 studies reported the first observations from ice-covered Tibetan lakes, indicating the
71 major role of solar radiation in their thermal regime (Wang et al., 2021). Water
72 temperatures in Lakes Bangong Co and Nam Co constantly increased during the ice-
73 covered period, with a stronger increase in shallower Bangong Co (Lazhu et al., 2021).
74 Observations in meromictic Dagze Co Lake demonstrated stable temperatures in the
75 early ice-covered period start warming only in the late ice-covered period, conditioned
76 by the high water salinity (Wang et al., 2014; Lazhu et al., 2021). Salinity has a strong
77 influence on the temperature and mixing regime of all three abovementioned lakes, by
78 altering their density stratification and vertical heat transport. Among freshwater lakes
79 in the TP, Ngoring Lake is the largest one (Kirillin et al. 2017; Wen et al. 2022). Kirillin
80 et al. (2021) found strong solar radiation under ice cover heating the entire lake water
81 column to the maximum freshwater density temperature (~ 3.98 °C, T_{md}) more than a
82 month before the ice breakup—the situation never found in lowland freshwater lakes.
83 As a result, strong heat release from water to the ice base turned into the major factor
84 governing the ice melt, with the water temperature under ice achieving 6 °C. This
85 radiation-dominated regime, differing dramatically from the typical heat budget known
86 from earlier studies on ice-covered lakes, does not fall under the framework of the
87 Winter I/Winter II classification, nor can be characterized in terms of
88 cryomictic/cryostratified conditions. Quantification of the resulting heat balance and
89 thermal stratification characteristic of alpine conditions is the subject of the present
90 study.

91 Due to the harsh environment of the TP and difficulties in collecting field
92 observations, numerical models are often used to investigate phenomena and
93 mechanisms of TP lakes. At present, the widely used lake models are the FLake model
94 and the lake scheme coupled in the CLM (Community Land Model), CoLM (Common
95 Land Model), and WRF (Weather Research and Forecasting Model) (Lazhu et al., 2016;
96 Wen et al., 2016; Fang et al., 2017; Dai et al., 2018; Huang et al., 2019; Song et al.,
97 2020; Wu et al., 2021). However, for computational efficiency, winter dynamics in these
98 highly-parameterized lake models are represented in a rather simplified way, lacking
99 the detailed mechanisms of heating by radiation and resulting vertical heat transports
100 across the water column (Lazhu et al., 2016; Wen et al., 2016; Huang et al., 2019). As
101 an alternative, we adopt for this study a “classical” two-equation turbulence modeling
102 approach proving its reliability in decades of studies on the environmental turbulent
103 fluid dynamics. The one-dimensional model LAKE implements the approach in
104 application to lake dynamics and was applied previously to different lakes (Stepanenko
105 et al., 2011, 2016; Guseva et al., 2016). We combine modeling with in situ observations
106 from Ngoring Lake, data on weather forcing and remote sensing to: (i) test the ability
107 of a one-dimensional lake model LAKE to simulate temperature and stratification

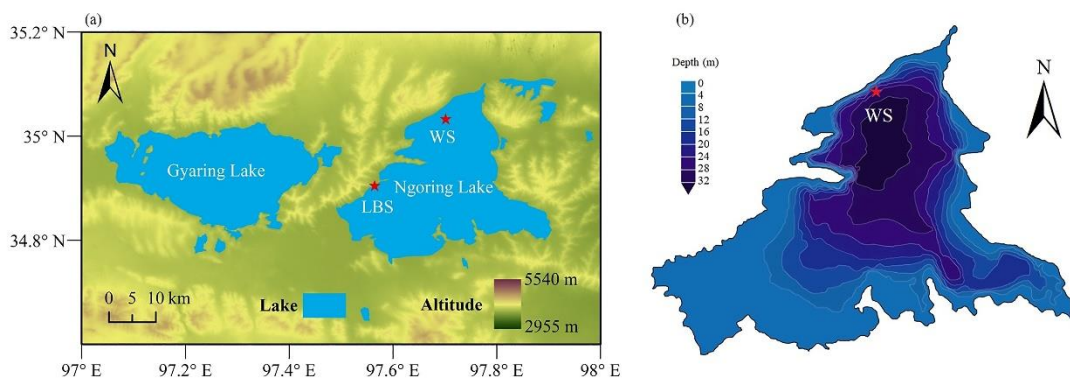
108 driven by intense solar heating in ice-covered Lake Ngoring; (ii) conduct series of
109 sensitivity experiments aimed at revealing the role of meteorological forcing and ice
110 optical properties in lake temperature and mixing regime; and (iii) reveal the effects of
111 temperature distribution before ice breakup on lake heat storage and lake- atmosphere
112 heat transfer.

113

114 2 Study area and data

115 2.1 Study area

116 Ngoring Lake (34.76-35.08° N, 97.53-97.90° E, Fig. 1) is located in the western
117 valley of Maduo County on the eastern TP, with an average lake surface elevation of
118 4274 m a.s.l. It is the largest freshwater lake in the Yellow River source region with a
119 salinity of about 0.27 g kg⁻¹ (Shen et al., 2012). It has a surface area of 610 km², a
120 maximum depth of 32 m, and an average depth of 17 m. The pH is 8.49 and there are
121 very few fish in the lake. Aquatic plants grow only in the riparian area. The lake
122 thermally stratifies in summer and is covered by ice from late November or early
123 December to late April (Wen et al., 2016). According to observational data from 1953
124 to 2016 at Maduo station (34.9° N, 98.2° E) of the China Meteorological Administration,
125 the average annual precipitation was 322.4 mm, mostly concentrated from May to
126 September. The average annual air temperature was -3.53 °C. The maximum air
127 temperature was 24.3 °C occurred on July 20, 2006, and the minimum air temperature
128 was -48.1 °C occurred on January 2, 1978.



129

130 **Figure 1. (a) Location and (b) bathymetry of Ngoring Lake. (b) is adapted from**
131 **Kirillin et al., 2021. The pentagrams denote the lake border station (LBS) and**
132 **water temperature measurement site (WS).**

133

134

135 **2.2 Data**

136 **2.2.1 Observational data: LBS station and WS site**

137 The long-term automatic lake border station (LBS, 34.91° N, 97.55° E, Fig. 1) was
138 installed in October 2012, with an altitude of 4282 m a.s.l., providing meteorological
139 forcing data: wind speed at 10 m, air temperature, specific humidity and air pressure at
140 2 m, downward shortwave (SR) and longwave radiation (LR) at 1.5 m from September
141 2015 to September 2016 (Li et al., 2020). The detailed information about site
142 configuration and measured quantities are referred to in Li et al. (2015b) and Wen et al.
143 (2016). The precipitation was obtained from the daily value data set (V3.0) at Maduo
144 station of Chinese surface climate data (<http://data.cma.cn>).

145 The water temperature measurement site (WS, 35.03° N, 97.70° E, Fig. 1) was
146 located in the northern of Ngoring Lake, where the total water depth was about 26.5 m.
147 The multi-layer water temperature observation system consisted of 16 self-recording
148 RBR SOLO water temperature probes with a precision of 0.01 °C. The sampling
149 distance and time intervals were 1 m and 10 minutes, respectively.

150

151 **2.2.2 MODIS lake surface temperature**

152 The 8-day L3 global lake surface temperature product (MYD11C2) was derived
153 from the data of Moderate Resolution Imaging Spectroradiometer (MODIS) and was
154 used to evaluate the simulated results. MODIS offers long-term daily global coverage
155 data with high spatial resolution. This product provides an 8-day combined radiative
156 surface temperature at approximately 10:30 and 22:30 LT (local time), which is the
157 satellite transit time. The resolution is 0.05° latitude/longitude (5600 m at the equator)
158 for Climate Modeling Grid (CMG) (<https://ladsweb.nascom.nasa.gov/search>) (Wan et
159 al., 2004).

160

161 **2.2.3 ERA5-Land data**

162 ERA5-Land is produced as an enhanced global dataset for the land component of
163 the fifth generation of European ReAnalysis (ERA5) by the European Centre for
164 Medium-Range Weather Forecasts (ECMWF), framed within the Copernicus Climate
165 Change Service (C3S) of the European Commission. It is available for ERA5-Land
166 hourly record for about 40 years from 1981 to the present. Expediently, ERA5-Land
167 has an enhanced horizontal resolution of 9 km (~0.08°) compared to ERA5 (31 km) and
168 ERA-Interim (80 km) (<https://cds.climate.copernicus.eu/cdsapp#!/dataset/reanalysis->

169 era5-land?tab=form) (Hersbach et al., 2020; Muñoz-Sabater et al., 2021).

170 ERA5-Land data is applied for a comparative analysis of warming mechanisms
171 and thermal conditions in Tibetan ice-covered lakes against those in the Arctic. The
172 reanalysis forcing data for the geographical position 69.05° N, 20.83° E was adopted as
173 “typical” arctic weather conditions. Northern Fennoscandia is covered by several lakes
174 characterized by the longest ice-covered period in Western Europe. The largest of these
175 lakes, Kilpisjärvi, has a similar morphometrical feature to Ngoring (average depth 19.5
176 m, maximum depth 57 m, surface area 37 km²). The lake has been intensively studied
177 in the last decades (Kirillin et al., 2015, 2018; Leppäranta et al., 2017, 2019). Its under-
178 ice water temperature remained stable during winter from 1992 to 1993 (Tolonen, 1998).
179 In the following, model experiments forced by the ERA5 weather data (1992-1993) for
180 the Arctic refer to “Kilpisjärvi” runs.

181

182 **3 Methods**

183 **3.1 LAKE model**

184 The one-dimensional model LAKE, simulating thermodynamic, hydrodynamic,
185 and biogeochemical processes, is used to solve the horizontally averaged transfer of
186 gases, heat, salts, and momentum in an enclosed water body (Stepanenko et al., 2011,
187 2016). The vertical heat diffusion is simulated, and the penetration of solar radiation
188 into the water ice, snow, and bottom sediments layers (Heiskanen et al., 2015; Cao et
189 al., 2020) is taken into account. The exchange between the water and the inclined
190 bottom is modeled explicitly because the model equations have been averaged over
191 horizontal sections of the water body. The 2nd order κ - ϵ parametrization of turbulence
192 is applied (Stepanenko et al., 2016).

193

194 **3.1.1 Heat transfer in water body**

195 The water temperature is calculated according to the one-dimensional thermal
196 diffusion equation:

$$\begin{aligned} 197 \quad c_w \rho_w \frac{\partial T_w}{\partial t} &= -c_w \rho_w \frac{1}{A} \int_{\Gamma_A} T_w (u_h \cdot n) dl + \frac{1}{Ah^2} \frac{\partial}{\partial \xi} \left(A_w K_T \frac{\partial T_w}{\partial \xi} \right) - \frac{1}{Ah} \frac{\partial AS}{\partial \xi} + \\ 198 \quad \frac{1}{Ah} \frac{\partial A}{\partial \xi} [S_b(\xi) + F_{iz,b}(\xi)] &+ \frac{dh}{dt} \frac{\xi}{h} \frac{\partial T_w}{\partial \xi}, \quad (1) \end{aligned}$$

199 where c_w is water specific heat, ρ_w is water density, T_w is water temperature, $h(t)$ is
200 lake depth, t is time, $\xi = z/h$ is a normalized vertical coordinate ($z \in [0, h]$), $z = 0$ is
201 located at the free water surface of the lake, S is downward shortwave radiation, A_w is

202 the z-dependent cross-sectional area of water, K_T is thermal diffusivity coefficient
 203 equal to the sum of molecular and turbulent diffusivities, $S_b(\xi)$ is shortwave radiation
 204 flux, $F_{i,z,b}$ is soil heat flux at the level z , n is an outer normal vector to the boundary Γ_A
 205 of the horizontal cross-section A and u_h is horizontal vector in water (Stepanenko et al.,
 206 2016; Guseva et al., 2016).

207

208 3.1.2 Heat transfer in ice cover

209 When the air temperature decreases below 0 °C and the surface water temperature
 210 drops to the freezing point, the initial ice cover forms. When the net radiation of the
 211 lake is positive, the ice melts continuously until the ice thickness declines to zero. The
 212 general heat conduction equation in ice cover follows the equation:

$$213 \quad c_i \rho_i \frac{\partial T_i}{\partial t} = c_i \rho_i \frac{\xi}{h_i} \frac{dh_i}{dt} \frac{\partial T_i}{\partial \xi} - c_i \rho_i \frac{1}{h_i} \frac{dh_{i0}}{dt} \frac{\partial T_i}{\partial \xi} - \frac{1}{h_i} \frac{\partial S}{\partial \xi} + \frac{1}{A_i h_i^2} \frac{\partial}{\partial \xi} \left(A_i \lambda_i \frac{\partial T_i}{\partial \xi} \right) + \frac{1}{A_i h_i} \frac{\partial A_i}{\partial \xi} F_{T,b} -$$

$$214 \quad L \rho_i \frac{dp}{dt}, \quad (2)$$

215 where c_i is ice specific heat, ρ_i is ice density, T_i is ice temperature, λ_i is ice thermal
 216 conductivity, h_i is ice thickness, $\frac{dh_{i0}}{dt}$ is the increment of ice thickness on its surface,
 217 $F_{T,b}$ is the heat flux at the ice-sediment boundary, A_i is the z-dependent cross-sectional
 218 area of the ice cover determined by the basin morphometry, L is the latent heat of water
 219 and p is ice porosity (Stepanenko et al., 2019). The last term to the right-hand side
 220 presents heat of phase transition of salty water in ice pores.

221 The penetration of solar radiation into the medium is calculated using the Beer-
 222 Lambert law (Stepanenko and Lykossov, 2005; Stepanenko et al., 2019):

$$223 \quad S(\xi) = S(0) \exp(-a_e h \xi), \quad (3)$$

224 where a_e is the medium extinction coefficient. To solve the temperature in Eq. (1 & 2),
 225 it is necessary to specify the top and bottom boundary conditions and provide the
 226 method to calculate the heat flux at each depth z . The atmospheric turbulent heat flux
 227 schemes are based on the Monin-Obukhov similarity theory (Stepanenko et al., 2016).

228 When the lake is covered by ice, the temperatures of the bottom layer of ice and
 229 the top layer of water are equal and fixed to the melting/freezing point temperature
 230 (Stepanenko et al., 2019), which is calculated by the following formula:

$$231 \quad T_{mp} = -C * \left| \partial T_{mp} / \partial C \right|, \quad (4)$$

232 where T_{mp} is the melting/freezing point temperature (°C), C is salinity at the water-
 233 ice interface, $\left| \partial T_{mp} / \partial C \right| = 66.7$ °C is assumed constant.

234 Based on the study by Leppäranta (2014), the albedo regulates the surface energy

235 budget, and the extinction coefficient controls the vertical distribution of radiation
 236 energy in the medium. In the LAKE model, the albedo of water (A_w) is 0.06, and the
 237 snow extinction coefficient (E_s) decreases with increased snow density. Snow
 238 accumulation in the Ngoring Lake area is almost zero. Therefore, only A_i , E_i , and E_w
 239 are analyzed in this study. Version 2.3 called LAKE2.3 is used in this article.

240

241 **3.2 Methods to evaluate the model accuracy**

242 The indexes to evaluate accuracy of the model are the root mean square error
 243 ($RMSE$), $BIAS$, and correlation coefficient (CC):

$$244 \quad RMSE = \sqrt{\frac{1}{n} \sum_{j=0}^n (m_j - o_j)^2} , \quad (5)$$

$$245 \quad BIAS = \bar{m} - \bar{o} , \quad (6)$$

$$246 \quad CC = \frac{\text{Cov}(M,O)}{\sqrt{\text{Var}(M)\text{Var}(O)}} , \quad (7)$$

247 where m_j and o_j represent the simulations and observations. \bar{m} and \bar{o} are the
 248 corresponding average values. $\text{Var}(M)$ and $\text{Var}(O)$ are the variances of observed and
 249 simulated values, respectively. $\text{Cov}(M, O)$ is the covariances.

250

251 **3.3 Calculation method of heat storage**

252 The heat storage evolution in water is calculated by the following formulation:

$$253 \quad Q = c_w \rho_w \sum_{k=1}^n T_k \Delta z_k , \quad (8)$$

254 where $c_w = 4192 \text{ J kg}^{-1} \text{ K}^{-1}$ and $\rho_w = 10^3 \text{ kg m}^{-3}$, n is the layer number, Δz_k is depth
 255 interval between two successive layers and T_k (K) is the average temperature in layer k
 256 (Nordbo et al., 2011; Gan and Liu, 2020).

257

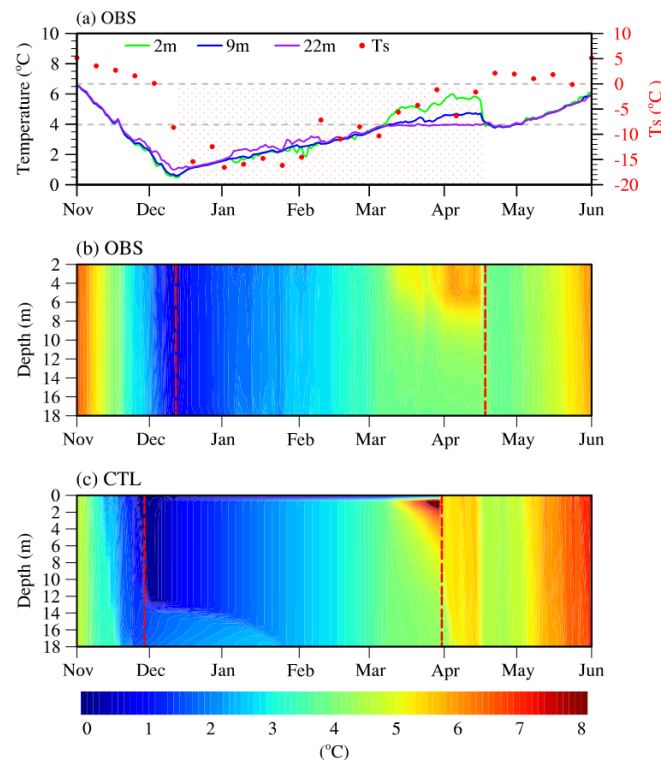
258 **4 Characteristic analysis of water temperature and local climate in two lakes**

259 **4.1 Characteristics of water temperature**

260 It is pointed out that the under-ice water temperature from 2015 to 2016 in Ngoring
 261 Lake rose continuously during the entire ice-covered period according to observations
 262 (Wang et al., 2021; Kirillin et al., 2021). In November, the lake mixed evenly with slight
 263 oscillation ($<1 \text{ }^\circ\text{C}$ between 2 m and 22 m) and water temperature decreased gradually

264 until the lowest point of 0.47 °C at 2 m on December 12, the lake froze up completely
 265 (Fig. 2a). Meanwhile, the air temperature at 2 m fell to -7.79 °C. Ngoring Lake is mostly
 266 covered only by bare ice in winter due to drought, less precipitation and snow. In the
 267 early ice-covered phase (from December 12 to March 7), the whole lake mixed
 268 completely because solar radiation penetrated ice and heated the upper water, which
 269 was warm ($< T_{md}$), heavy and sinking (Fig. 2b) (Kirillin et al., 2012). In parallel, water
 270 temperature continued to warm until reached T_{md} on March 7 (Fig. 2a).

271 In the late ice-covered stage (from March 7 to April 18), the lake stratified. On the
 272 one hand, owing to solar radiation strengthened, on the other hand, since radiation
 273 absorption of water decayed with depth based on the Beer-Lambert law. Water
 274 temperature increased at the rate of 0.052 °C d⁻¹ in the layers from 2 m to 6 m, which
 275 was more rapid than the early stage of 0.035 °C d⁻¹. On April 18, the ice melted entirely
 276 as well water temperature rose to 5.83 °C at 2 m while remaining at T_{md} below 9 m.
 277 After that, full mixing took place rapidly because the lake warmed gaining heat from
 278 the sun and atmosphere as a result of ice breaking up (Fig. 2b).

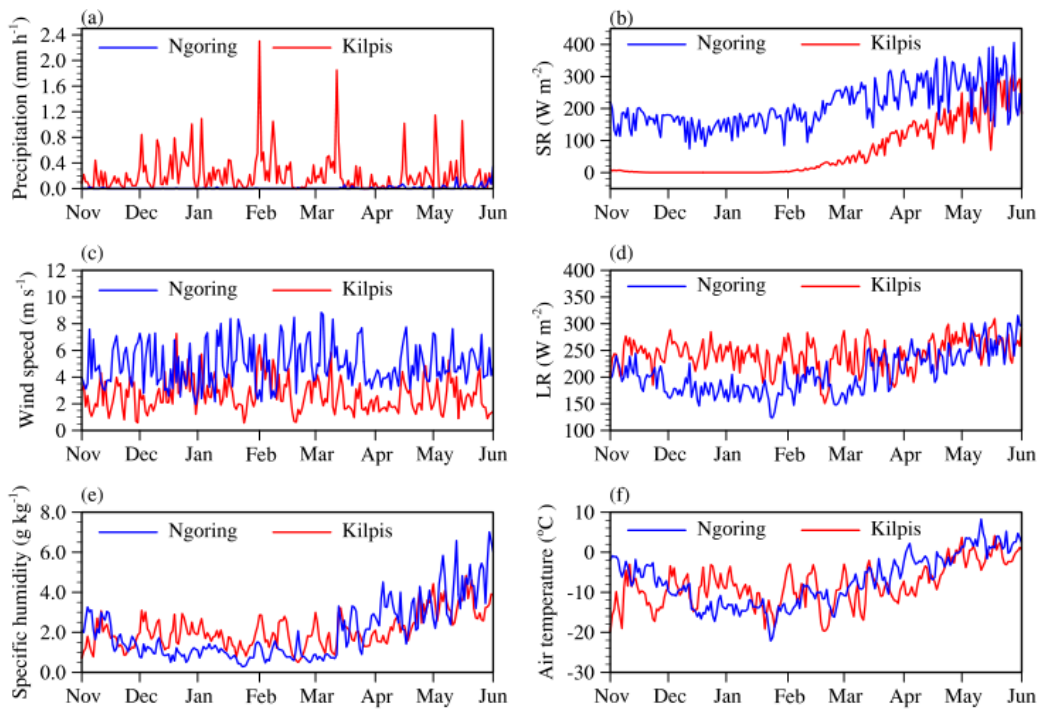


279
 280 **Figure 2. (a) The daily average water temperature observations of Ngoring Lake**
 281 **at the surface (Ts), 2 m, 9 m, and 22 m from November 1, 2015 to June 1, 2016. Ts**
 282 **is MODIS lake surface temperature. The gray reference lines denote 3.98 °C and**
 283 **0 °C, respectively. The pink shaded area denotes ice-covered period. The water**
 284 **temperature profile (b) observed and (c) simulated in CTL. The ice-covered period**
 285 **is represented between the two red dashed lines.**

286 **4.2 Local climate: Tibet vs. Kilpisjärvi**

287 The daily averages of meteorological variables between Tibet and Kilpisjärvi were
288 shown in Fig. 3, the ranges and averages of that during the ice-covered period (from
289 December 12 to April 18 based on Ngoring Lake) were compared (Table 1). The
290 average differences in air temperature, specific humidity, and downward LR were -
291 0.42 °C, -0.38 g kg⁻¹, and 41.9 W m⁻², respectively. The wind speed of Tibet was 1.7
292 times that of Kilpisjärvi, and the downward SR in Tibet of 199.41 W m⁻² was stronger
293 than in Kilpisjärvi of 40.46 W m⁻². The precipitation was a multiple of 0.037 in Tibet
294 than that in Kilpisjärvi.

295 On the whole, there were few differences in air temperature, specific humidity, and
296 downward LR in the two regions. Nevertheless, there was much lower precipitation,
297 much higher downward SR and wind speed in Tibet. Surface pressure was not
298 considered in this study since the little effect on water temperature.



299

300 **Figure 3. Comparison of daily average values of the meteorological variables for**
301 **Tibet from 2015 to 2016 and for Kilpisjärvi from 1992 to 1993. (a) precipitation,**
302 **(b) downward SR, (c) wind speed, (d) downward LR, (e) specific humidity, and (f)**
303 **air temperature. The “Ngoring” represents the Tibet region and the “Kilpis”**
304 **represents Kilpisjärvi region.**

305

306

307

308 **Table 1.** Ranges and averages of the meteorological variables of Tibet (2015-2016)
 309 compared with Kilpisjärvi (1992-1993) during the ice-covered period (12.12-4.18).

Meteorologic variables	Tibet		Kilpisjärvi	
	Range	Average	Range	Average
Precipitation (mm h ⁻¹)	< 0.072	0.0044	< 1.15	0.12
Downward SR (W m ⁻²)	73.98-356.29	199.41	< 186.84	40.46
Wind speed (m s ⁻¹)	1.95-8.85	4.93	0.56-7.28	2.83
Downward LR (W m ⁻²)	123.92-271.60	191.73	150.61-289.59	233.62
Specific humidity (g kg ⁻¹)	0.29-4.52	1.40	0.50-3.23	1.78
Air temperature (°C)	-22.16-2.24	-10.25	-19.69-2.01	-9.83

310

311 **5 Simulation setup**

312 To reveal the mechanism of water temperature rising during ice-covered period in
 313 Ngoring Lake and its further influences, one control simulation (CTL) and 27
 314 sensitivity simulations (SIM) depending on CTL were set in this study (Table 2).

315

316 **5.1 Setup in CTL**

317 The depth was set as 26.5 m, measured at the WS point, and divided vertically into
 318 35 layers. The simulation period was from September 2015 to September 2016. The
 319 initial vertical profile of water temperature, mixed layer, and the bottom temperature
 320 were set following the observations (Fig. 2b). The albedos of snow and ice and the
 321 extinction coefficients of ice and water were set as $A_s = 0.7$, $A_i = 0.25$, $E_i = 2.5 \text{ m}^{-1}$, and
 322 $E_w = 0.15 \text{ m}^{-1}$ based on previous investigations (Lei et al., 2011; Li et al., 2018, 2020;

323 Shang et al., 2018). The input driving meteorological variables were air pressure, wind
 324 speed, specific humidity, air temperature, precipitation, downward SR, and LR. The
 325 forcing data and model run interval was 30 minutes and 15 seconds respectively.

326

327 5.2 Setup in SIM

328 To explore the influence of a single meteorological variable, SIM_* simulations
 329 were set up. The symbol * is SR, Precip, LR, U, Tair, or q in Kilpisjärvi. These scenarios
 330 were quite artificial because these variables are closely correlated. Despite that, these
 331 sensitivity simulations can shed light on the influence of local climate on lake
 332 temperature evolution during ice-covered period.

333 To discuss the effect of main physical parameters, SIM_# simulations were set up,
 334 the sign # represented the values of A_i , E_i , or E_w . SIM_E* (* equal to 1, 2, or 3) is set
 335 for exploring the effects of three different initial water temperature profiles before ice
 336 breakup on the lake heat storage and heat fluxes.

337

338 **Table 2.** Names, explanations, and amounts of all experiments.

Experiment name	Experiment explanation	Amount
CTL	Control simulation	1
SIM_*		
(* represents meteorological variables)	The simulation when the * variable is replaced by that of Kilpisjärvi.	6
SIM_#		
(# represents values of A_i , E_i or E_w)	The simulation when the corresponding physical variable is equal to #, respectively.	18
SIM_E*		
(* represents 1, 2, and 3)	The simulation when using three different initial temperature profiles before ice melting based on CTL.	3

339

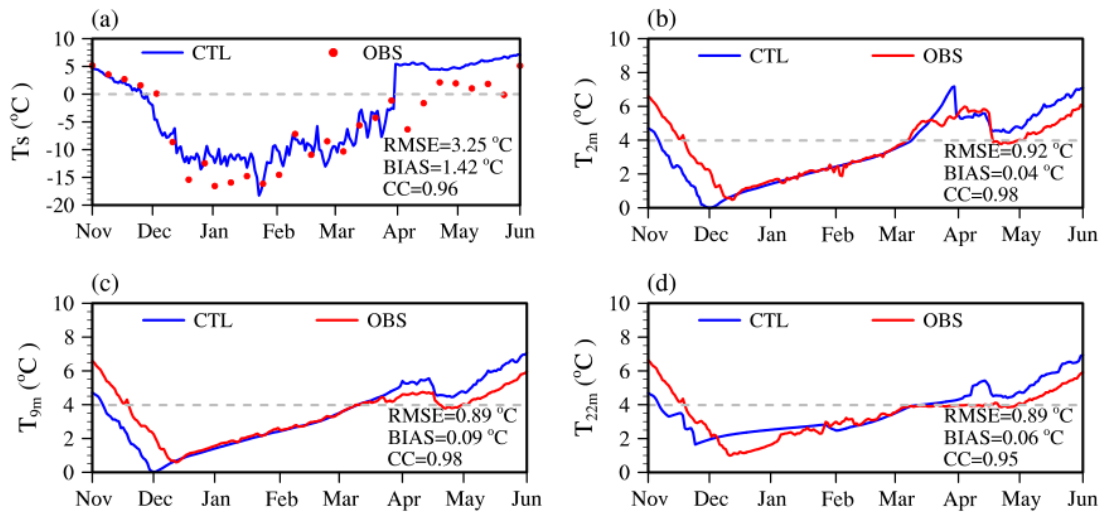
340 6 Simulation results

341 6.1 Model validation

342 The simulations in CTL were relatively consistent with the observations (Fig. 2b,c),

343 even though the whole ice season advanced by about 15 days than observed. Water
 344 temperature was a little higher in CTL than that in the observations from mid-March to
 345 late May. The deviation was greater in the deep water. The simulated temperature
 346 warmed faster and higher by 1 °C than the observed value after ice melted.

347 The results were evaluated by calculating *RMSE*, *BIAS*, *CC* between simulated and
 348 observed water temperature at the lake surface (T_s), 2 m, 9 m and 22 m (Fig. 4). The
 349 *CC* in each layer was equal to even greater than 0.95, and the *CC* in 2 m and 9 m are as
 350 high as 0.98, even though *RMSE* and *BIAS* of lake surface were 3.25 °C and 1.42 °C,
 351 respectively. The T_s *RMSE* was largely due to the uncertainty of MODIS lake surface
 352 temperature (Donlon et al., 2002; Tavares et al., 2019). The *BIAS* absolute values in the
 353 internal lake were less than 0.01 °C, and *RMSE* was less than 0.95 °C. More important,
 354 the under-ice temperature warming phenomenon was reproduced reasonably.



355

356 **Figure 4. The daily average water temperature observed and simulated in CTL of**
 357 **(a) the surface (T_s), (b) 2 m, (c) 9 m, (d) 22 m in Ngoring Lake from November**
 358 **2015 to June 2016. The dotted line represents T_{md} 3.98 °C.**

359

360 6.2 Influences of local climate on water temperature

361 To explore the influences of local climate on water temperature, six simulations
 362 SIM_* (* represents 6 meteorological variables, Table 2) were designed. The 3 m water
 363 temperature was typically selected to analyze since water temperature at different
 364 depths varied consistently over time.

365 SIM_SR was the simulation when the Kilpisjärvi downward SR was substituted
 366 for that in Tibet. During the ice-covered period, the downward SR difference between
 367 CTL (199.41 W m⁻²) and SIM_SR (40.46 W m⁻²) was 158.95 W m⁻². In the sensitivity
 368 simulation SIM_SR, the 3 m water temperature was stable keeping in the range of 0-

369 0.1 °C (Fig. 5a). The ice formation date was earlier and the ice-breaking date delayed,
370 which led to the growth of the whole ice season. The mixed layer depth increased (Fig.
371 5d). Consequently, the strong downward SR on the TP generated the under-ice water
372 warming in Ngoring Lake.

373 In the simulation SIM_Precip, the Tibet precipitation was replaced by that in
374 Kilpisjärvi. In the sensitivity experiment SIM_Precip, the 3 m water temperature fixed,
375 then increased but did not exceed T_{md} in the early ice cover stage (Fig. 5a). The
376 stratification and temperature maximum center disappeared in late March, and the lake
377 was fully mixed (Fig. 2c,5g). Because the average precipitation in SIM_Precip (0.12
378 mm h⁻¹) was approximately 30 times larger than that in CTL (0.0044 mm h⁻¹) during
379 ice-covered period, more solar radiation was reflected and absorbed by snow due to
380 more snowfall accumulation. Thus, the high precipitation damped the water
381 temperature rise.

382 In SIM_LR simulation, the downward LR in Kilpisjärvi superseded that in Tibet.
383 The average downward LR was 233.62 W m⁻² in SIM_LR, which was stronger than
384 that in CTL (191.73 W m⁻²) during ice-covered period. The 3 m water temperature still
385 warmed as well the complete ice melting time of late February was ahead. The heat was
386 transferred from lake to atmosphere because of lower air temperature after ice breakup.
387 The water temperature underwent a cooling process (2 °C) until reaching a new
388 equilibrium with atmosphere (Fig. 5b). Compared with the CTL, water mixing in the
389 ice-covered period was more uniform, the stratification in late March was weakened,
390 and the temperature maximum center advanced about 15 days (Fig. 5e).

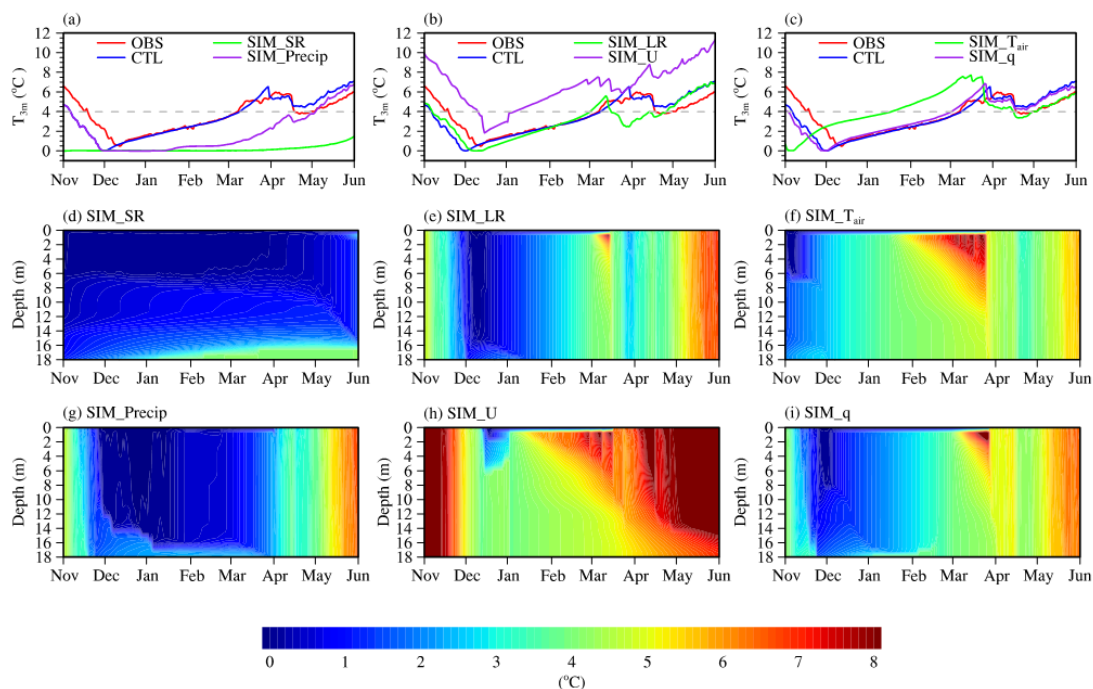
391 In SIM_U simulation, the wind speed of Kilpisjärvi was substituted for that of Tibet.
392 The wind speed in SIM_U (2.83 m s⁻¹) was weaker than that in CTL (4.93 m s⁻¹) for the
393 ice cover period. In the sensitivity experiment SIM_U, the 3 m water temperature kept
394 rising, but it was about 3 °C higher than that in CTL during the whole simulation period
395 (Fig. 5b). Due to the decrease in wind speed, the mixed layer depth was reduced, and
396 the lake stratification was more stable (Fig. 5h).

397 In SIM_T_{air} simulation, the air temperature of Kilpisjärvi was replaced by that of
398 Tibet. The average air temperature difference between SIM_T_{air} (-9.83 °C) and CTL (-
399 10.25 °C) was negligible (0.42 °C). In the sensitivity experiment SIM_T_{air}, the water
400 temperature decreased more quickly, and in late October, the lake froze no longer
401 releasing heat into atmosphere. The lake stratification was enhanced, and the water
402 temperature maximum center was ahead about 10 days (Fig. 5c,f).

403 In SIM_q simulation, the specific humidity of Kilpisjärvi was substituted for Tibet.
404 The difference in specific humidity between SIM_q and CTL was 0.38 g kg⁻¹ during

405 ice-covered period. In the sensitivity experiment SIM_q, the simulations were
 406 coincidental to that in CTL, and thus the specific humidity had little effect on the water
 407 temperature (Figs. 5c,i).

408 In conclusion, the stronger downward SR and lower precipitation in TP played
 409 positive roles in the water temperature warming during the ice-covered period in
 410 Ngoring Lake. Less downward LR, lower air temperature, and larger wind speed did
 411 not change the warming trend but affected the warming amplitude and rate. Specific
 412 humidity had no significant influence.



413

414 **Figure 5.** The simulated 3 m daily average water temperature in (a) (d) SIM_{SR},
 415 (a) (g) SIM_{Precip}, (b) (e) SIM_{LR}, (b) (h) SIM_U, (c) (f) SIM_{T_{air}}, (c) (i) SIM_q
 416 sensitivity experiments from November 2015 to June 2016 are compared with the
 417 CTL and the observation, and the change of vertical stratification is shown. The
 418 dotted line represents 3.98 °C.

419

420 6.3 Influences of main physical parameters on water temperature

421 The radiation transfer, which depended on the albedo and extinction coefficient,
 422 played a decisive role in the water temperature. Only influences of A_i , E_i , and E_w on
 423 water temperature simulation were discussed with sensitivity experiments due to less
 424 snow in Tibet. According to previous observations, A_i has observed on TP was mostly
 425 less than 0.12, and the albedo of clear blue ice was only 0.075 (Li et al., 2018). The
 426 range of A_i without snow cover was set as 0.1-0.8 with an interval of 0.1 in SIM_{A_i}

427 experiments.

428 E_i has not been observed on TP, but surveys in Finnish lakes show that the value of
429 bare ice varies between 1-4 m^{-1} , while the value of snow-covered ice can reach 5 m^{-1}
430 (Lei et al., 2011). In SIM_ E_i simulations, E_i was equal to 1-5 m^{-1} with an interval of 1
431 m^{-1} .

432 For the E_w , Zolfaghari et al. (2017) found that the FLake model is particularly
433 sensitive at $E_w \leq 0.5 \text{ m}^{-1}$. Shang et al. (2018) observed that E_i varies from 0.11 to 0.67
434 m^{-1} in a few TP lakes. Therefore, the sensitivity simulations SIM_ E_w were designed in
435 which the E_w varied from 0.1 to 0.5 m^{-1} with an increment step of 0.1 m^{-1} . The
436 experimental settings are shown in Table 3.

437

438 **Table 3.** Numerical sensitivity simulations of parameters affecting the radiative transfer.

Parameter	CTL	SIM_ A_i	SIM_ E_i	SIM_ E_w
A_i	0.25	0.1/0.2/0.3/0.4/0.5 /0.6/0.7/0.8	0.25	0.25
E_i (m^{-1})	2.5	2.5	1.0/2.0/3.0/4.0 /5.0	2.5
E_w (m^{-1})	0.15	0.15	0.15	0.1/0.2/0.3/0.4 /0.5

439

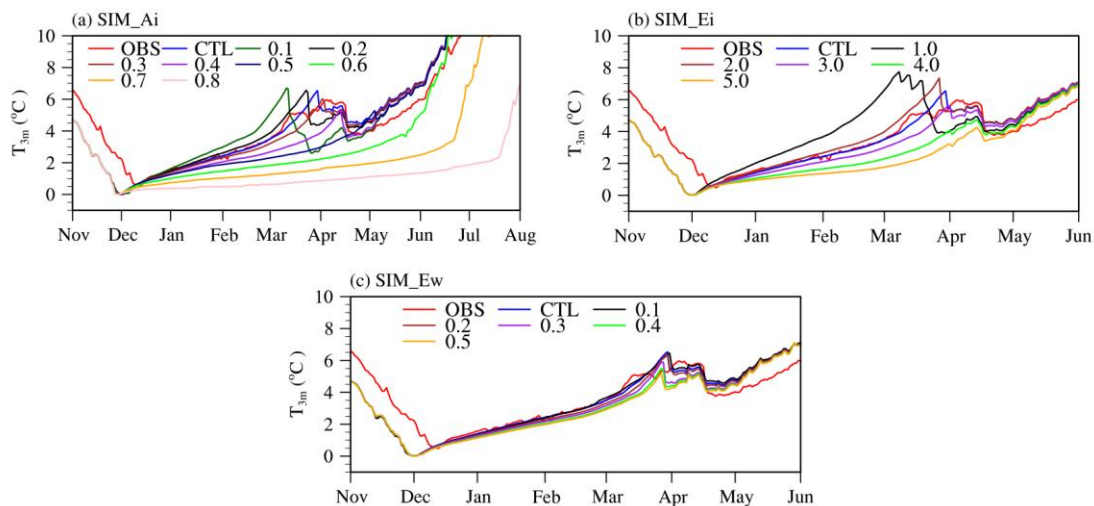
440 In the SIM_ A_i sensitivity experiment, the 3 m water temperature decreased
441 approximately 1 °C when ice albedo increased by 0.1. When the albedo grew to 0.80,
442 the water temperature warming decreased from 4 °C to 2 °C. The increase of ice albedo
443 did not affect the ice formation date but remarkably delayed the ice melting time,
444 accordingly prolonging the ice-covered period. When the albedo increased from 0.1 to
445 0.8, the ice-covered period was extended for 15-30 days for every 0.1 increase (Fig. 6a).

446 In the sensitivity experiment SIM_ E_i , the ice extinction coefficient changes did not
447 all make a continuous rising in water temperature, but the 3 m water temperature
448 decreased by 1-2 °C when ice extinction coefficient increased by 1 m^{-1} (Fig. 6b). The
449 ice absorbed more heat, and the less heat entered the lake water under ice due to the
450 larger ice extinction coefficient.

451 To further discuss influences of A_i and E_i on lake temperature during ice-covered
452 period. The period was divided into two stages Period-A and Period-B in CTL, SIM_ A_i .

453 Period-A ranged from freezing point to T_{md} , Period-B ranged from T_{md} to maximum
 454 temperature (T_m). The duration of Period-A is longer than that of Period-B, and the
 455 temperature heating rate in Period-B ($\sim 0.1 \text{ }^\circ\text{C d}^{-1}$) was 2.5 times greater than that of
 456 Period-A ($\sim 0.04 \text{ }^\circ\text{C d}^{-1}$). The reason was that lake completely covered by ice, and the
 457 inner lake evenly mixed in Period-A, while the ice thickness decreased and the radiation
 458 absorbed by the ice decreased in Period-B. The upper layer absorbed more heat than
 459 the deeper layer, and the upper water temperature increased rapidly. When A_i and E_i
 460 increased, the heating rate decreased and the duration increased in Period-A, the T_{max}
 461 decreased, the heating rate and duration fluctuate in Period-B. When $A_i \geq 0.6$, the
 462 heating rate during ice-covered period decreases and did not rise to T_{md} .

463 In the SIM_Ew sensitivity experiment, the water extinction coefficient had just a
 464 little influence on the winter water temperature, 3 m water temperature decreased with
 465 the increase of Ew (Fig. 6c). When only the extinction coefficient of water changed, the
 466 solar radiation entering the water through the ice is unchanged, and so the heat storage
 467 of the lake was unaffected. It's just that the heat distribution in the vertical direction is
 468 changed. The higher the extinction coefficient of water, the more heat was absorbed by
 469 the surface layer and the less heat reached the deep layer. The phenomenon that the 3
 470 m water temperature decreases with the extinction coefficient increasing becomes more
 471 and more obvious in the later stage of ice melting.



472

473 **Figure 6. Comparison of the 3m simulated daily average water temperature with**
 474 **the observed value under different (a) A_i , (b) E_i , (c) E_w .**

475

476 **6.4 Influences of water temperature on lake-atmosphere exchange**

477 The thermal conditions in an ice-covered lake just before ice melting have a
 478 significant influence on the air-lake energy exchange. To analyze the effects of lake

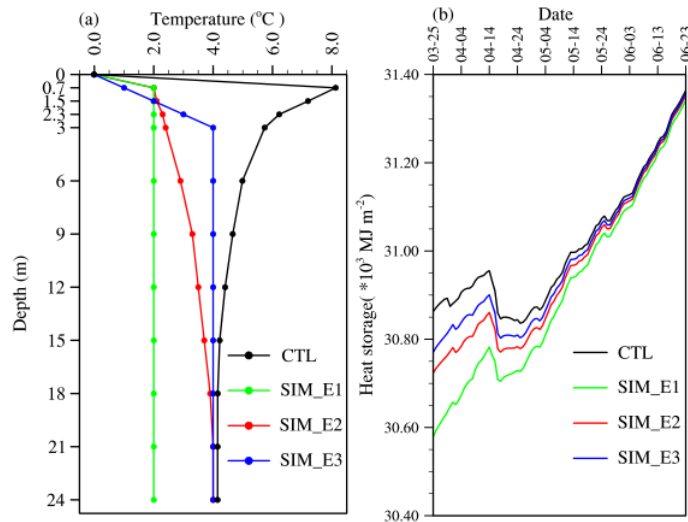
479 temperature characteristics on the atmosphere at ice melting, three experiments –
480 SIM_E1, SIM_E2, and SIM_E3 (Table 1) – were set up based on the CTL and the
481 observed lake temperature profile on March 25, 2016, 5 days before ice completely
482 melted (Fig. 7a). The characteristics of the initial water temperature profile were:

- 483 - SIM_E1. The stratification was weak, the first layer temperature was at the
484 melting point, and, from the second layer down, the water temperature was set
485 as 2 °C corresponding to Bangong Co (Wang et al., 2014).
- 486 - SIM_E2. The lake was strongly stratified. The first layer was at the melting
487 point, and the temperature increased linearly reaching T_{md} at the bottom,
488 corresponding to Valkea-Kotinen Lake (Bai et al., 2016).
- 489 - SIM_E3. The temperature of the first layer was at the melting point, and the
490 temperature gradually increased with the depth from the second layer to the
491 middle layer, and the temperature in the middle layer increased to T_{md}
492 corresponding to Thrush Lake (Fang and Stefan, 1996).

493 In CTL, the first layer temperature equal to the freezing/melting point, and the
494 second layer reached the maximum temperature on March 25. The temperature became
495 lower with the deeper layer, until the temperature reached T_{md} .

496 With the different initial temperature profiles, the heat storage was different after
497 ice breakup, and the difference persisted for about two months (Fig. 7b). In CTL, from
498 March 30 to March 31 when ice melted completely, the lake heat storage ranged from
499 30893.02 MJ m⁻² to 30874.51 MJ m⁻², and the heat released was 18.51 MJ m⁻². In the
500 three experiments, from April 1 to April 2 when ice melted completely, the lake heat
501 storage changed from 30657.51 MJ m⁻² to 30651.67 MJ m⁻² in SIM_E1, from 30781.07
502 MJ m⁻² to 30769.91 MJ m⁻² in SIM_E2, and from 30833.28 MJ m⁻² to 30822.42 MJ m⁻²
503 in SIM_E3, and the heat release was 5.84 MJ m⁻², 11.16 MJ m⁻², and 10.86 MJ m⁻²,
504 respectively (Fig. 7b).

505 The heat released was in the form of sensible heat and latent heat, accounting for
506 0.060% (CTL), 0.019% (SIM_E1), 0.036% (SIM_E2), and 0.035% (SIM_E3) of the
507 ice-covered heat storage, respectively. As the initial lake temperature profiles were
508 different before ice complete melting, the ice melted earlier and faster with the higher
509 lake temperature. The lake heat storage increased from March 25 to May 24, and the
510 heat release rate was different under different circumstances. After late May, the heat
511 balance between the lake and the atmosphere was the same, and so the heat storage
512 basically stayed equally after that.

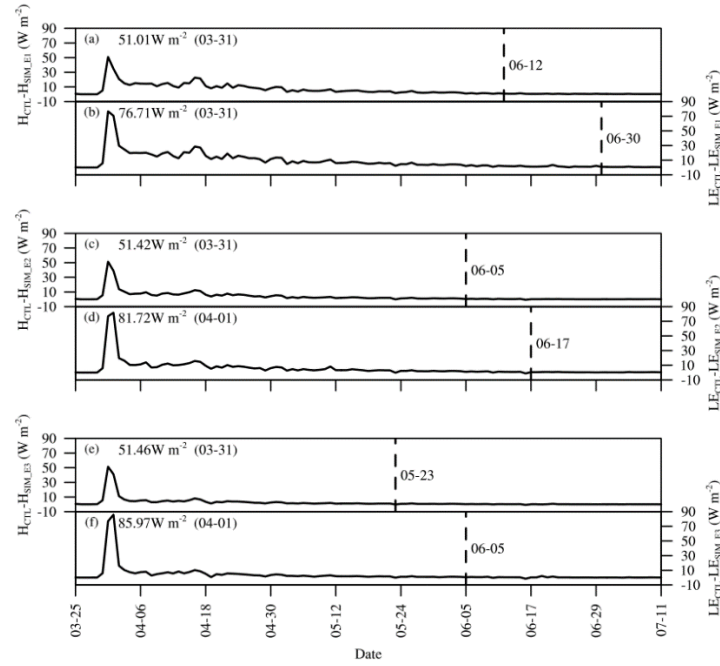


513

514 **Figure 7. (a) The initial water temperature profiles in the model are set on March**
 515 **25, 2016, and the corresponding daily average (b) lake heat storage is simulated.**
 516 **SIM_E1, SIM_E2, and SIM_E3 are three different sensitivity simulations.**

517

518 The lake surface temperature also affected the sensible and latent heat release,
 519 whose differences were calculated between CTL and the three experimental simulations
 520 (Fig. 8). The influence of different initial water temperature profiles started on March
 521 31, that is, when the ice had melted completely in CTL, and when the sensible and latent
 522 differences between CTL and three experimental simulations were less than 0.1 W m^{-2}
 523 for three consecutive days, we judged that the influence had ended. The maximum
 524 differences of the sensible heat (51.0 W m^{-2}) and latent heat (76.7 W m^{-2}) between
 525 SIM_E1 and CTL appeared on March 31 and ended on June 12 and 30, respectively
 526 (Fig. 8a). In SIM_E2 the corresponding numbers were 51.4 W m^{-2} (March 31 to June
 527 5) for sensible heat and 81.7 W m^{-2} (April 1 to June 17) for latent heat (Fig. 8b), and in
 528 SIM_E3 they were 51.5 W m^{-2} (March 31 to May 23) for sensible heat and 86.0 W m^{-2}
 529 (April 1 to June 5) for latent heat (Fig. 8c). Compared with the three lake temperature
 530 experiments, the heating characteristics of Ngoring Lake made the heat release higher
 531 and faster during ice breakup. The duration of heat release difference was from 59 (to
 532 May 23) to 97 (to June 30) days, and for the latent heat release, the situation lasted
 533 about 12-18 days longer than for the sensible heat release.



534

535 **Figure 8. The daily average difference between the sensitivity sensible and latent**
 536 **heat and the CTL under three different initial water temperature profiles in**
 537 **SIM_E1, SIM_E2, and SIM_E3.**

538

539 **7 Conclusions**

540 The analysis demonstrates a significant increase in lake temperature during the ice-
 541 covered period in Ngoring, the largest freshwater lake on the Tibetan Plateau (TP), with
 542 water temperatures exceeding the freshwater maximum density value T_{md} . The heating
 543 is governed by strong solar radiation, the factor differing alpine lakes on the TP from
 544 the low-altitude northern lakes with similar winter air temperature patterns. The one-
 545 dimensional lake model LAKE2.3 successfully captured the major mechanisms of
 546 warming and vertical thermal stratification during the ice-covered period. Compared
 547 with MODIS surface temperature data, the *BIAS*, *RMSE*, and *CC* were 1.42 °C, 3.25 °C,
 548 and 0.96, respectively. The absolute values of *BIAS* and *RMSE* were less than 0.1 °C
 549 and 1 °C in 2 m, 9 m, 14 m, and 22 m. The *CC* of simulated and observed water
 550 temperature at 2 m, 9 m, and 14 m were as high as 0.98, and the *CC* of simulated and
 551 observed water temperature at 22 m was 0.95.

552 Sensitivity simulations with perturbed local climate data confirmed the decisive
 553 role of subsurface solar radiation in the water temperature rise and demonstrated strong
 554 negative feedback with winter precipitation amount. The downward longwave radiation,
 555 air temperature, and wind speed had only a minor influence on the water temperature.

556 The warming rates and, as a result, the duration of the ice-covered period was

557 sensitive to the physical ice properties: ice albedo and light extinction coefficient both
558 reduced the amount of the subsurface solar radiation. An increase in the albedo of ice
559 reduced the rising trend of water temperature and prolonged the ice season. At the
560 critical albedo of 0.6, the lake water warming decreased obviously and temperature
561 remained stable no more than 3.98 °C. The extinction coefficient of water had just a
562 minor effect on water temperature under the ice.

563 An important consequence of the under-ice solar heat accumulation consisted in
564 increased sensible and latent heat releases in the subsequent open-water phase.
565 According to the model results, the effects on the surface fluxes of Ngoring Lake lasted
566 for 59-97 days after the ice melt and increased the upward latent and sensible surface
567 heat fluxes up to $\sim 80 \text{ W m}^{-2}$ and $\sim 50 \text{ W m}^{-2}$, respectively. Herewith, the phenomenon
568 of under-ice solar heating may have a significant effect on the land-atmosphere
569 interaction on regional scales and has to be accounted for in coupled climate models.

570

571 *Data availability.* The daily precipitation data from Chinese surface stations are
572 available for purchase from the China Meteorological Data Service Center (CMDC,
573 <http://data.cma.cn/en/>). The MODIS LST product is available from National
574 Aeronautics and Space Administration (NASA) (<https://earthdata.nasa.gov/>). ERA5-
575 Land data is available with funding from the European Union's Copernicus Climate
576 Change Service (<https://cds.climate.copernicus.eu/>). Lake temperature data of Ngoring
577 Lake in 2015 and 2016 were uploaded to Zenodo by Georgiy Kirillin
578 (<http://doi.org/10.5281/zenodo.4750910>). The weather observation data of Ngoring
579 Lake can be obtained from the website (<https://nimbus.igb-berlin.de/index.php/s/Moqxgn29DbNFyr8>). The latest version of LAKE model source
580 code is available at Zenodo: <https://zenodo.org/record/6353238#.YjCSXi1eNTY> .

582

583 *Author contributions.* MW and LW conceived the study. MW performed the modeling
584 with contributions from VS, LW, and ZL. YZ, RN, and LY processed some data. MW,
585 LW, ML, and GK analyzed the model output. MW wrote the paper, with contributions
586 from all co-authors.

587

588 *Competing interests.* The authors declare that they have no conflict of interest.

589

590 *Acknowledgments.* This study was supported by the National Key Research and
591 Development Program of China (2019YFE0197600) and CAS "Light of West China"
592 Program (E129030101, Y929641001). Victor Stepanenko was supported by Russian
593 Ministry of Science and Higher Education, agreement No. 075-15-2019-1621.

594 **References**

- 595 Bai, Q. X., Li, R. L., Li, Z. J., Leppäranta, M., Arvola, L. and Li, M.: Time-series
596 analyses of water temperature and dissolved oxygen concentration in Lake Valkea-
597 Kotinen (Finland) during ice season, *Ecol Inform*, 36, 181-189, doi:
598 10.1016/j.ecoinf.2015.06.009, 2016.
- 599 Brown, L. C. and Duguay, C. R.: The fate of lake ice in the North American Arctic, *The*
600 *Cryosphere*, 5, 869-892, doi: 10.5194/tc-5-869-2011, 2011.
- 601 Cao, X. W., Lu, P., Leppäranta M., Arvola L., Huotari J., Shi X. H., Li G. Y. and Li Z.
602 J.: Solar radiation transfer for an ice-covered lake in the central Asian arid climate zone,
603 *Inland Waters*, 11, 89-103, doi: 10.1080/20442041.2020.1790274, 2020.
- 604 Dai, Y. J., Wei, N., Huang, A. N., Zhu, S. G., Shangguan, W., Yuan, H., Zhang, S. P. and
605 Liu, S. F.: The lake scheme of the Common Land Model and its performance evaluation
606 (in Chinese), *Chin Sci Bull*, 63, 3002-3021, doi: 10.1360/n972018-00609, 2018.
- 607 Dauginis, A. A. and Brown, L. C.: Recent changes in Pan-Arctic sea ice, lake ice, and
608 snow on/off timing, *The Cryosphere*, 15, 4781-4805, doi: 10.5194/tc-2021-52, 2021.
- 609 Dokulil, M. T.: Predicting summer surface water temperatures for large Austrian lakes
610 in 2050 under climate change scenarios, *Hydrobiologia*, 731, 19-29, doi:
611 10.1007/s10750-013-1550-5, 2013.
- 612 Donlon, C. J., Minnett, P. J., Gentemann, C., Nightingale, T. J., Barton, I. J., Ward, B.,
613 and Murray, M. J.: Toward improved validation of satellite sea surface skin temperature
614 measurements for climate research, *J. Clim.*, 15, 353–369, doi:
615 10.1175/15200442(2002)015<0353:TIVOSS>2.0.CO;2, 2002.
- 616 Efremova, T., Palshin, N. and Zdorovenov, R.: Long-term characteristics of ice
617 phenology in Karelian lakes, *EST J EARTH SCI*, 62, 33-41, doi: 10.3176/earth.2013.04,
618 2013.
- 619 Fang, N., Yang, K., Lazhu, Chen, Y. Y., Wang, J. B. and Zhu, L. P.: Research on the
620 application of WRF-lake Modeling at Nam Co Lake on the Qinghai-Tibetan Plateau,
621 *Plateau Meteorology*, 36, 610-618, doi: 10.7522/j.issn.1000-0534.2016.00038, 2017.
- 622 Fang, X. and Stefan, H. G.: Long-term lake water temperature and ice cover
623 simulations/measurements, *Cold Reg Sci Technol*, 24, 289-304, 1996.
- 624 Gan, G. J. and Liu, Y. B.: Heat storage effect on evaporation estimates of China's largest
625 freshwater lake, *J. Geophys*, 125, 1-14, doi: 10.1029/2019jd032334, 2020.
- 626 Grant, L., Vanderkelen, I., Gudmundsson, L., Tan, Z., Perroud, M., Stepanenko, V.,
627 Debolskiy, A. V., Droppers, B., Janssen, A. B., Woolway, R. I., Choulga, M., Balsamo,
628 G., Kirillin, G., Schewe, J., Zhao, F., Valle, I. V., Golub, M., Pierson, D., Marcé, R.,
629 Seneviratne, S. I. and Thiery, W.: Attribution of global lake systems change to
630 anthropogenic forcing, *Nat. Geosci.*, 14, 1-6, doi: 10.1038/s41561-021-00833-x, 2021.
- 631 Guseva, S., Stepanenko, V., Shurpali, N., Biasi, C., Marushchak, M. E. and Lind, S. E.:

632 Numerical simulation of methane emission from Subarctic Lake in Komi Republic
633 (Russia), *Geography, Environment, Sustainability*, 9, 58-74, doi: 10.15356/2071-
634 9388_02v09_2016_05, 2016.

635 Hardenbicker, P., Viergutz, C., Becker, A., Kirchesch, V., Nilson, E. and Fischer, H.:
636 Water temperature increases in the river Rhine in response to climate change, *Reg
637 Environ Change*, 17, 299-308, doi: 10.1007/s10113-016-1006-3, 2016.

638 Heiskanen, J. J., Mammarella, I., Ojala, A., Stepanenko, V., Erkkilä, K. M., Miettinen,
639 H., Sandström, H., Eugster, W., Leppäranta, M., Järvinen, H., Vesala, T. and Nordbo,
640 A.: Effects of water clarity on lake stratification and lake-atmosphere heat exchange, *J.
641 Geophys*, 120, 7412-7428, doi: 10.1002/2014jd022938, 2015.

642 Hersbach, H., Bell, B., Berrisford, P., Hirahara, S., Horányi, A., Muñoz-Sabater, J.,
643 Nicolas, J., Peubey, C., Radu, R., Schepers, D., Simmons, A., Soci, C., Abdalla, S.,
644 Abellan, X., Balsamo, G., Bechtold, P., Biavati, G., Bidlot, J., Bonavita, M., Chiara, G.,
645 Dahlgren, P., Dee, D., Diamantakis, M., Dragani, R., Flemming, J., Forbes, R., Fuentes,
646 M., Geer, A., Haimberger, L., Healy, S., Hogan, R. J., Hólm, E., Janisková, M., Keeley,
647 S., Laloyaux, P., Lopez, P., Lupu, C., Radnoti, G., Rosnay, P., Rozum, I., Vamborg, F.,
648 Villaume, S. and Thépaut, J. N.: The ERA5 global reanalysis, *Q J R Meteorol Soc*, 146,
649 1999-2049, doi: 10.1002/qj.3803, 2020.

650 Huang, A. N., Lazhu, Wang, J. B., Dai, Y. J., Yang, K., Wei, N., Wen, L. J., Wu, Y., Zhu,
651 X. Y., Zhang, X. D. and Cai, S. X.: Evaluating and improving the performance of three
652 1-D lake models in a large deep lake of the central Tibetan Plateau, *J. Geophys*, 124,
653 3143-3167, doi: 10.1029/2018JD029610, 2019.

654 Kirillin, G. B., Aslamov, I., Kozlov, V., Zdorovenov, R., and Granin, N.: Turbulence
655 in the stratified boundary layer under ice: observations from Lake Baikal and a new
656 similarity model, *Hydrol. Earth Syst. Sci.*, 24, 1691-1708, doi: 10.5194/hess-24-1691-
657 2020, 2020.

658 Kirillin, G. B., Aslamov, I., and Leppäranta, M.: Turbulent mixing and heat fluxes under
659 lake ice: the role of seiche oscillations, *Hydrol. Earth Syst. Sci.*, 22, 6493-6504, doi:
660 10.5194/hess-22-6493-2018, 2018.

661 Kirillin, G. B., Leppäranta, M., Terzhevik, A., Granin, N., Bernhardt, J., Engelhardt, C.,
662 Efremova, T., Golosov, S., Palshin, N., Sherstyankin, P., Zdorovenova, G. and
663 Zdorovenov, R: Physics of seasonally ice-covered lakes: a review, *Aquat Sci*, 74, 659-
664 682, doi: 10.1007/s00027-012-0279-y, 2012.

665 Kirillin, G. B., Wen, L. J. and Shatwell, T.: Seasonal thermal regime and climatic trends
666 in lakes of the Tibetan highlands, *Hydrol Earth Syst Sci*, 21, 1895-1909, doi:
667 10.5194/hess-21-1895-2017, 2017.

668 Kirillin, G. B., Forrest, A. L., Graves, K. E., Fischer, A., Engelhardt, C. and Laval, B.
669 E.: Axisymmetric circulation driven by marginal heating in ice-covered lakes, *Geophys*

670 Res Lett, 42, 2893-2900, doi: 10.1002/2014gl062180, 2015.

671 Kirillin, G. B., Shatwell, T. and Wen, L. J.: Ice-covered lakes of Tibetan Plateau as solar
672 heat collectors, *Geophys. Res. Lett.*, 48, 1-12, doi: 10.1029/2021gl093429, 2021.

673 Lazhu, Yang, K., Hou, J. Z., Wang, J. B., Lei, Y. B., Zhu, L. P., Chen, Y. Y., Wang, M.
674 D. and He, X. G.: A new finding on the prevalence of rapid water warming during lake
675 ice melting on the Tibetan Plateau, *Sci. Bull.*, 66, 2358-2361, doi:
676 10.1016/j.scib.2021.07.022, 2021.

677 Lazhu, Yang, K., Wang, J. B., Lei, Y. B., Chen, Y. Y., Zhu, L. P., Ding, B. H. and Qin,
678 J.: Quantifying evaporation and its decadal change for Lake Nam Co, central Tibetan
679 Plateau, *J. Geophys.*, 121, 7578-7591, doi: 10.1002/2015jd024523, 2016.

680 Lei, R. B., Leppäranta, M., Erm, A., Jaatinen, E. and Pärn, O.: Field investigations of
681 apparent optical properties of ice cover in Finnish and Estonian lakes in winter 2009,
682 *EST J EARTH SCI*, 60, 50-64, doi: 10.3176/earth.2011.1.05, 2011.

683 Leppäranta, M.: Freezing of lakes and the evolution of their ice cover, Germany:
684 Springer Science & Business Media, 2014.

685 Leppäranta, M., Lindgren, E. and Shirasawa, K.: The heat budget of Lake Kilpisjärvi
686 in the Arctic tundra, *Hydrology Research*, 48, 969-980, doi: 10.2166/nh.2016.171, 2017.

687 Leppäranta, M., Lindgren, E., Wen, L. J. and Kirillin, G.: Ice cover decay and heat
688 balance in Lake Kilpisjärvi in Arctic tundra, *J Limnol*, 78, doi:
689 10.4081/jlimnol.2019.1879, 2019.

690 Li, G. C., Liu, Z. G., Zhang, M., Li, J., Pi, K., Xiong, Y. and Xu, J.: A preliminary study
691 of effects of warming on the nutrients dynamic in sediment of hypereutrophic shallow
692 lake, *Acta Ecologica Sinica*, 35, 4016-4025, doi: 10.5846/stxb201309102244, 2015a.

693 Li, Z. G., Ao, Y. H., Lyu, S. H., Lang, J. H., Wen, L. J., Stepanenko, V., Meng, X. H.
694 and Zhao, L.: Investigation of the ice surface albedo in the Tibetan Plateau lakes based
695 on the field observation and MODIS products, *J Glaciol*, 64, 506-516, doi:
696 10.1017/jog.2018.35, 2018.

697 Li, Z. G., Lyu, S. H., Ao, Y. H., Wen, L. J., Zhao, L. and Wang, S. Y.: Long-term energy
698 flux and radiation balance observations over Lake Ngoring, Tibetan Plateau, *Atmos Res*,
699 155, 13-25, doi: 10.1016/j.atmosres.2014.11.019, 2015b.

700 Li, Z. G., Lyu, S. H., Wen, L. J., Zhao, L., Ao, Y. H. and Meng, X. H.: Study of freeze-
701 thaw cycle and key radiation transfer parameters in a Tibetan Plateau lake using
702 LAKE2.0 model and field observations, *J Glaciol*, 45, 1-16, doi: 10.1017/jog.2020.87,
703 2020.

704 Muñoz-Sabater, J., Dutra, E., Agustí-Panareda, A., Albergel, C., Arduini, G., Balsamo,
705 G., Boussetta, S., Choulga, M., Harrigan, S., Hersbach, H., Martens, B., Miralles, D.
706 G., Piles, M., Rodríguez-Fernández, N. J., Zsoter, E., Buontempo, C. and Thépaut, J.-
707 N.: ERA5-Land: A state-of-the art global reanalysis dataset for land applications, *Earth*

708 Syst. Sci. Data, 1-50, doi: 10.5194/essd-2021-82, 2021.

709 Nordbo, A., Launiainen, S., Mammarella, I., Leppäranta, M., Huotari, J., Ojala, A. and
710 Vesala, T.: Long-term energy flux measurements and energy balance over a small boreal
711 lake using eddy covariance technique, *J. Geophys.*, 116, 1-17, doi:
712 10.1029/2010jd014542, 2011.

713 Ramp, C., Delarue, J., Palsboll, P. J., Sears, R. and Hammond, P. S.: Adapting to a
714 warmer ocean--seasonal shift of baleen whale movements over three decades, *PLoS*
715 *One*, 10, 1-15, doi: 10.1371/journal.pone.0121374, 2015.

716 Rösner, R. R., Müller-Navarra, D. C. and Zorita, E.: Trend analysis of weekly
717 temperatures and oxygen concentrations during summer stratification in Lake Plußsee:
718 A long-term study, *Limnol. Oceanogr.*, 57, 1479-1491, doi: 10.4319/lo.2012.57.5.1479,
719 2012.

720 Shang, Y. X., Song, K. S., Jiang, P., Ma, J. H., Wen, Z. D. and Zhao, Y.: Optical
721 absorption properties and diffuse attenuation of photosynthetic active radiation for
722 inland waters across the Tibetan Plateau, *Journal of Lake Sciences*, 30, 802-811, doi:
723 10.18307/2018.0322, 2018.

724 Sharma, S., Blagrove, K., Magnuson, J. J., O'Reilly, C. M., Oliver, S., Batt, R. D.,
725 Magee, M. R., Winslow, L. and Woolway, R. I.: Widespread loss of lake ice around the
726 Northern Hemisphere in a warming world, *Nature Clim. Change.*, 9, 227-231, doi:
727 10.1038/s41558-018-0393-5, 2019.

728 Sharma, S., Meyer, M. F., Culpepper, J., Yang, X., Hampton, S., Berger, S. A., Brousil,
729 M. R., Fradkin, S. C., Higgins, S. N., Jankowski, K. J., Kirillin, G., Smits, A. P.,
730 Whitaker, E. C., Yousef, F. and Zhang, S.: Integrating Perspectives to Understand Lake
731 Ice Dynamics in a Changing World, *J Geophys Res-bioge*, 125, 1-18, doi:
732 10.1029/2020jg005799, 2020.

733 Shen, D. F., Li, S. J., Jiang, Y. J. and Chen, W.: Water environment characteristics and
734 regional climate response of typical lakes in Yellow River headwater area, *J. Arid*
735 *Environ.*, 26, 91-97, doi: 10.13448/j.cnki.jalre.2012.07.030, 2012.

736 Song, X. Y., Wen, L. J., Li, M. S., Du, J., Su, D. S., Yin, S. C. and Lv, Z.: Comparative
737 study on applicability of different lake models to typical lakes in Qinghai-Tibetan
738 Plateau, *Plateau Meteorology*, 39, 213-225, doi: 10.7522/j.issn.1000-0534.2019.00102,
739 2020.

740 Stepanenko, V., Mammarella, I., Ojala, A., Miettinen, H., Lykosov, V. and Vesala, T.:
741 LAKE 2.0: a model for temperature, methane, carbon dioxide and oxygen dynamics in
742 lakes, *Geosci Model Dev*, 9, 1977-2006, doi: 10.5194/gmd-9-1977-2016, 2016.

743 Stepanenko, V. and Lykosov, V. N.: Numerical modeling of heat and moisture transfer
744 processes in a system lake soil, *Russ. Meteorol. Hydrol.*, 3, 95-104, doi: 2005.

745 Stepanenko, V., Machul'skaya, E. E., Glagolev, M. V. and Lykosov, V. N.: Numerical

746 modeling of methane emissions from lakes in the permafrost zone, *IZV ATMOS*
747 *OCEAN PHY+*, 47, 252-264, doi: 10.1134/s0001433811020113, 2011.

748 Stepanenko, V., Repina, I. A., Ganbat, G. and Davaa, G.: Numerical simulation of ice
749 cover of saline lakes, *IZV ATMOS OCEAN PHY+*, 55, 129-138, doi:
750 10.1134/s0001433819010092, 2019.

751 Tavares, M., Cunha, A., Motta-Marques, D., Ruhoff, A., Cavalcanti, J., Fragoso, C.,
752 Martín Bravo, J., Munar, A., Fan, F. and Rodrigues, L.: Comparison of methods to
753 estimate Lake-Surface-Water temperature using Landsat 7 ETM+ and MODIS imagery:
754 Case study of a large shallow subtropical lake in Southern Brazil, *Water*, 11, 1-21, doi:
755 10.3390/w11010168, 2019.

756 Tolonen, A.: Application of a bioenergetics model for analysis of growth and food
757 consumption of subarctic whitefish *Coregonus lavaretus* (L.) in Lake Kilpisjärvi,
758 Finnish Lapland, *Hydrobiologia*, 390, 153–169, doi: 10.1023/A:1003525008870, 1998.

759 Wan, W., Long, D., Hong, Y., Ma, Y. Z., Yuan, Y., Xiao, P. F., Duan, H. T., Han, Z. Y.
760 and Gu, X. F.: A lake data set for the Tibetan Plateau from the 1960s, 2005, and 2014,
761 *Sci. Data*, 3, 1-13, doi: 10.1038/sdata.2016.39, 2016.

762 Wan, Z., Zhang, Y., Zhang, Q. and Li, Z. L.: Quality assessment and validation of the
763 MODIS global land surface temperature, *Int J Remote Sens*, 25, 261-274, doi:
764 10.1080/0143116031000116417, 2004.

765 Wang, M. D., Hou, J. Z. and Lei, Y. B.: Classification of Tibetan lakes based on
766 variations in seasonal lake water temperature, *Chinese Science Bulletin*, 59, 4847-4855,
767 doi: 10.1007/s11434-014-0588-8, 2014.

768 Wang, M. X., Wen, L. J., Li, Z. G. and Su, D. S.: Study on the warming characteristics
769 during the ice-covered period of Ngoring Lake in the Qinghai-Xizang Plateau, *Plateau*
770 *Meteorology*, 40, 965-976, doi: 10.7522/j.issn.1000-0534.2020.00112, 2021.

771 Weitere, M., Vohmann, A., Schulz, N., Linn, C., Dietrich, D. and Arndt, H.: Linking
772 environmental warming to the fitness of the invasive clam *Corbicula fluminea*, *Glob*
773 *Chang Biol*, 15, 2838-2851, doi: 10.1111/j.1365-2486.2009.01925.x, 2010.

774 Wen, L. J., Lyu, S. H., Kirillin, G., Li, Z. G. and Zhao, L.: Air–lake boundary layer and
775 performance of a simple lake parameterization scheme over the Tibetan highlands,
776 *Tellus A*, 68, 1-15, doi: 10.3402/tellusa.v68.31091, 2016.

777 Wen, L. J., Wang, C., Li, Z. G., Zhao, L., Lyu, S. H. and Chen, S. Q.: Thermal Responses
778 of the Largest Freshwater Lake in the Tibetan Plateau and Its Nearby Saline Lake to
779 Climate Change, *Remote Sens*, 14, 1-19, doi: 10.3390/rs14081774, 2022.

780 Wu, Y., Huang, A. N., Lazhu, Yang, X. Y., Qiu, B., Zhang, Z., Q. and Zhang X., D.:
781 Numerical study of the thermal structure and circulation in a large and deep dimictic
782 lake over Tibetan Plateau, *J. Geophys*, 126, 1-22, doi: 10.1029/2021jc017517, 2021.

783 Yang, B., Wells, M. G., McMeans, B. C., Dugan, H. A., Rusak, J. A., Weyhenmeyer, G.

784 A., Brentrup, J. A., Hrycik, A. R., Laas, A., Pilla, R. M., Austin, J. A., Blanchfield, P. J.,
785 Carey, C. C., Guzzo, M. M., Lottig, N. R., MacKay, M. D., Middel, T. A., Pierson, D.
786 C., Wang, J. and Young, J. D.: A new thermal categorization of ice-covered lakes,
787 *Geophys. Res. Lett.*, 48, 1-11, doi: 10.1029/2020gl091374, 2021.
788 Zhang, G. Q., Luo, W., Chen, W. F. and Zheng, G. X.: A robust but variable lake
789 expansion on the Tibetan Plateau, *Sci. Bull.*, 64, 1306-1309, doi:
790 10.1016/j.scib.2019.07.018, 2019.
791 Zolfaghari, K., Duguay, C. R. and Kheyrollah Pour, H.: Satellite-derived light
792 extinction coefficient and its impact on thermal structure simulations in a 1-D lake
793 model, *Hydrol Earth Syst Sci*, 1-36, doi: 10.5194/hess-2016-82, 2017.
794